Ultracold neutron accumulation in a superfluid-helium converter with magnetic multipole reflector

O. Zimmer[1] and R. Golub[2]
[1]*Institut Laue Langevin, 38042 Grenoble, France*
[2]*Department of Physics, North Carolina State University, Raleigh, North Carolina 27695, USA*
(Received 7 July 2014; revised manuscript received 10 March 2015; published 2 July 2015)

We analyze the accumulation of ultracold neutrons (UCNs) in a superfluid-helium converter vessel surrounded by a magnetic multipole reflector. We solved the spin-dependent rate equation, employing formulas valid for adiabatic spin transport of trapped UCNs in mechanical equilibrium. Results for saturation UCN densities are obtained in dependence of order and strength of the multipolar field. The addition of magnetic storage to neutron optical potentials can increase the density and energy of the low-field-seeking UCNs produced and serves to mitigate the effects of wall losses on the source performance. It also can provide a highly polarized sample of UCNs without need to polarize the neutron beam incident on the converter. This work was performed in preparation of the UCN source project SuperSUN at the Institut Laue–Langevin.

DOI: 10.1103/PhysRevC.92.015501 PACS number(s): 07.20.Mc, 29.25.Dz

I. INTRODUCTION

Mirror reflection of neutrons is an effect of the neutron optical potential which is mainly due to coherent s-wave scattering of neutrons by atomic nuclei in condensed matter [1]. Ultracold neutrons (UCNs), which were first produced in Dubna [2] and in Munich [3], have energy sufficiently low to become totally reflected under any angle of incidence. This peculiar property enables experimentalists to store them in "neutron bottles" made of suitable materials with small cross sections for neutron absorption and providing well depths up to about 300 neV [4,5]. Storage time constants of many hundreds of seconds and the possibility to employ also magnetic fields and gravity for trapping and manipulation have made UCNs a versatile tool to investigate various phenomena of fundamental physics complementary to experiments at high-energy particle accelerators [6–8].

Among the recent experiments with UCNs features a first demonstration of gravity resonance spectroscopy with the goal being to search for deviations from Newton's gravity law at the micrometer length scale [9], searches for "mirror dark matter" [10,11], a test of Lorentz invariance [12], searches for axion-like particles [13–15], and a demonstration of the effect of accelerated matter on the neutron wave [16] and of the stability of the Berry geometrical phase for spin-$\frac{1}{2}$ particles under the influence of noise fluctuations [17]. Earlier work with UCNs on the geometrical phase was published in Refs. [18,19], while its first demonstration with cold neutrons can be found in Ref. [20].

Long standing are the efforts to improve the accuracy of the weak axial-vector and vector coupling constants of the nucleon derived from precise values of the neutron lifetime [21–25] and the beta asymmetry [26–29]. Among other applications, these values are crucial input for calculations of weak reaction rates in big-bang nucleosynthesis and stellar fusion [30,31] and of the efficiency of neutrino detectors [32]. Also long standing is the search for a nonvanishing neutron electric dipole moment (EDM), which would violate the symmetries of parity (P) and time reversal (T) and thus via the CPT theorem also violate the combined symmetries of charge conjugation and parity (CP). This search was proposed already in 1950 by Purcell and Ramsey [33] and has become a prominent route to investigate new mechanisms of CP violation beyond the standard model's complex phase of the weak quark mixing Cabibbo–Kobayashi–Maskawa (CKM) matrix, and the matter-antimatter asymmetry in the universe [34]. At the present best level of sensitivity, still no EDM was observed [35]. Several projects are in preparation or underway with the goal to gain at least an order of magnitude in sensitivity [36–44] .

Most studies with UCNs are counting-statistics limited and will strongly profit from new UCN sources that are currently being developed in various laboratories around the world [45–54]. They are all based on the "superthermal" UCN production scheme proposed in 1975 by one of the authors together with Pendlebury [55], using either superfluid ^{4}He or solid deuterium as a medium for neutron conversion. Early milestones in the development of the latter were published in Refs. [56–58]. Here we focus on UCN production in a converter of superfluid ^{4}He installed at the end of a neutron guide, wherein neutrons with energy 1 meV and wavelength 0.89 nm may loose nearly their entire energy in single scattering events. At low temperature only few excitations are present in the helium that are able to scatter UCNs back to higher energies. With the vanishing absorption cross section of ^{4}He it becomes possible to accumulate UCNs within a converter with reflective boundaries before releasing them to an experiment at room temperature. While an earlier attempt to bring this technique to life was hampered by extraction losses (nonetheless producing record UCN densities for its time) [59], a more efficient method was developed recently by one of the authors together with his coworkers [47,60–62]. UCNs are extracted through a cold UCN valve and a short vertical UCN guide section, superseding lossy separation window, screens, and gaps for thermal insulation between the converter and the UCN guide of the earlier scheme. Work is in progress to bring the technique to maturity for a new user facility at the Institut Laue-Langevin (ILL), and in particular for performing a neutron-lifetime experiment using magnetic trapping [63–65]. Also other groups have recognized the potential advantages of a superfluid helium converter feeding UCNs to experiments at

room temperature [50,51], and in some experiments this type of converter is employed *in situ* [39,43,66].

The efficiency of an UCN accumulator at an external neutron beam relies on loss rates being sufficiently low. Most critical are those losses which occur when UCNs hit the walls of the converter vessel. They are proportional to the frequency of collisions and thus depend on the size and shape of the converter vessel. From transmission measurements through superfluid ^{4}He at 1.25 K, a mean-free path of 17 m was derived for the 0.89 nm neutrons most effective for UCN production [67]. Hence, the vessel can be made several meters long without significant reduction in UCN density. On the other hand, the lateral dimensions of the converter vessel should match the size of the available neutron beam and guide it to avoid dilution of the incident flux. The mean-free path of UCNs in a vessel with such geometry is therefore only on the order of 5 to 10 cm, leading to high typical frequencies of UCN wall collisions of 50 to 100 per second. It thus becomes challenging to obtain long UCN-storage time constants which, however, are a prerequisite for accumulation of a high saturated UCN density. Values measured for narrow vessels are normally well below 200 s. For instance, in a recent experiment on UCN production, a rather short storage time constant of 67 s was obtained for a vessel held at 0.7 K, which consisted of a 1-m-long 7×7 cm^2 tube of BeO with Be windows on each end and included a short pipe from stainless steel. That, nonetheless, a record UCN density was obtained demonstrates the potential of the method [60]. To the best of our knowledge the Cryo-EDM collaboration achieved with $\tau = 160$ s the so-far highest value for a helium converter enclosed within matter boundaries by using a 3-m-long tubular vessel with diameter 63 mm, made of Be coated copper and closed off by Be windows [39].

Magnetic trapping of UCNs offers a viable way for a drastic improvement of the storage properties of the converter vessel, ultimately limited only by the neutron lifetime $\tau_\beta \approx 880$ s. It relies on the potential energy $\pm\mu_n B$ of the neutron magnetic moment $\mu_n \approx 60$ neV/T in a magnetic field B. Suitable configurations of magnetic field gradients keep the low-field-seeking UCNs away from walls where otherwise the collisional losses occur. A group at NIST demonstrated storage-time constants consistent with the neutron lifetime within a helium converter equipped with a superconducting magnetic quadrupole UCN reflector [66,68]. The apparatus was designed to perform neutron-lifetime measurements, for which a complete suppression of UCN wall contacts is mandatory. On the other hand, for the sake of enhancing the output of a UCN source, combined magnetic and material trapping turns out to be particularly beneficial. In addition, the phase space for UCN accumulation can be much increased by using a higher multipole order.

In this paper we provide an analytic treatment of the rate equation for UCN production and storage in a superfluid-helium converter confined by material walls and surrounded by a magnetic mirror. We show that, by combining a converter vessel possessing good (but not exceptional) storage properties with a magnetic mirror of high multipole order, one may achieve a saturated UCN density close to the theoretical limit defined by an ideal experimental bottle, i.e., a square-well potential without an imaginary part. That the magnet needs to generate only part of the trapping potential is of great practical value for constructing a device using standard superconducting-wire technology.

II. RATE EQUATION AND SYSTEM DEFINITION

The temporal evolution of the spectral UCN density in a closed converter irradiated by the cold beam is governed by a simple rate equation. UCN production is characterized by a spectral rate density p that depends on the spectral flux of the incident beam, and a loss term is due to finite lifetime τ of UCNs in the converter,

$$\frac{dn(\epsilon_0,t)}{dt} = p(\epsilon_0) - \frac{n(\epsilon_0,t)}{\tau(\epsilon_0)}. \tag{1}$$

Here we label stored neutrons by their total energy ϵ_0, defined as their kinetic energy at the point of lowest potential energy in the trap. The quantities $n(\epsilon_0,t)$ and $p(\epsilon_0)$ denote the real space density and the spatial UCN production rate density, respectively, each per energy interval of a group of UCNs having total energy in the range $(\epsilon_0,\epsilon_0 + d\epsilon_0)$. The saturated spectral UCN density occurs when UCN losses balance UCN production for $t \gg \tau$ after having switched on the beam. It is given by

$$n_\infty(\epsilon_0) = p(\epsilon_0)\tau(\epsilon_0). \tag{2}$$

If one wants to fill a trap with UCNs up to the cutoff energy set by the trapping potential $V_{\rm trap}$, what matters is the saturated total UCN density which is obtained from

$$n_\infty = \int_0^{V_{\rm trap}} n_\infty(\epsilon_0)d\epsilon_0. \tag{3}$$

Many applications of UCN sources involve filling external traps with as many UCNs as possible, followed by a long time for holding or manipulation, during which the density in the source can be refreshed. Therefore, n_∞ is a useful parameter of the converter to be optimized.[1]

We consider a system as schematically shown in Fig. 1. A cylindrical converter vessel with diameter $2R$ is situated within a multipole magnet and illuminated homogeneously by a cold-neutron beam passing along the $r = 0$ axis. UCN accumulation takes place over a length $L \gg R$ between a beam window and a UCN valve fully immersed in the helium as in the apparatus described in Ref. [69]. Shown is a butterfly valve but different types may also be envisaged, such as an iris diaphragm valve. For experiments at room temperature, UCNs are released into a windowless extraction system with a short vertical guide section as described in Ref. [61].[2] In the

[1]For experiments involving external traps with poor storage properties it will be better to drain UCNs frequently from a partially charged source. However, also in this case a long UCN-storage-time constant is an asset because it will raise the time-averaged UCN content of the converter.

[2]It is also conceivable to place the UCN valve closer to (or within) the extraction guide. This would, however, considerably increase the

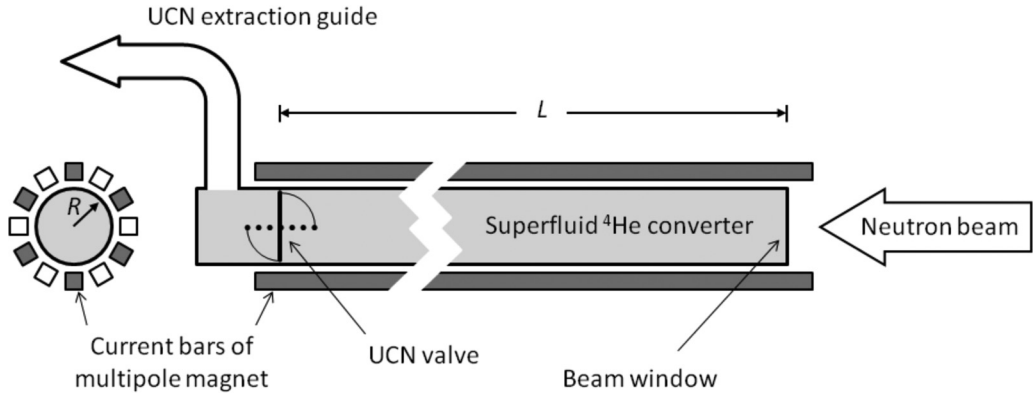

FIG. 1. Schematic of the UCN accumulator comprised of a superfluid ^{4}He converter with multipole magnet and system for UCN extraction. On the left a cut view is shown for $n = 12$; filled (open) squares indicate electric current flowing into (out of) the plane. The neutron optical potentials are V for the cylindrical inner surface over the length L, $\widetilde{V}$ at the beam window and at the UCN valve, respectively, $\geqslant \widetilde{V}$ for the UCN extraction system, and $V_{\rm He} \approx 18.5$ neV in the superfluid.

section for UCN accumulation the cylindrical wall possesses a neutron optical potential $V + iW$ [1,4,5], with

$$V = \frac{2\pi\hbar^2}{m_{\rm n}} \sum_l N_l b_l, \quad W = \frac{\hbar}{2} \sum_l N_l v \sigma_l(v), \tag{4}$$

where $m_{\rm n}$ is the neutron mass, N_l is the atomic number density of the nuclear species l with coherent bound neutron scattering length b_l, and $\sigma_l(v)$ is the loss cross section [the sum of cross sections for neutron capture and upscattering; v is the UCN velocity in the medium and $v\sigma_l(v)$ is usually constant over the whole UCN spectrum]. The beam window and the UCN valve are made of (or coated with) a material with neutron optical potential $\widetilde{V} + i\widetilde{W}$.

A radial n-polar magnetic field with modulus

$$B(r) = B_R \left(\frac{r}{R}\right)^{\frac{n}{2}-1} \tag{5}$$

can be generated as shown by using a regular arrangement of an even number of n straight current bars on the outer cylinder surface, with opposite current in adjacent bars (in practice one employs long racetrack coils). A neutron moving in such a field has a magnetic potential energy of

$$V_{\rm m}(r) = \pm V_{{\rm m}R} \left(\frac{r}{R}\right)^{\frac{n}{2}-1}, \quad V_{{\rm m}R} = |\mu_{\rm n}| B_R, \tag{6}$$

where the upper (lower) sign in this and all subsequent equations describes neutrons in the low-field-seeking (high-field-seeking) spin state, denoted by lfs and hfs in the sequel. Note that we assume adiabatic spin transport and thus neglect spin-flip transitions. It is an experimentally established fact that the validity of the adiabatic condition can be fulfilled better than needed for our purposes by using a weak bias field on the order of a few 10 mT along the axis of the multipole magnet. For instance, an octupole trap has provided UCN storage lifetimes on the order of 800 s. Losses occurred primarily due to UCNs hitting a teflon piston coated with Fomblin grease, which was used for axial closure of the trap [70]. A storage lifetime much closer to the neutron lifetime was attained in a 20-pole magnetic trap, in which UCNs were held without any wall collisions [71].

Due to addition of magnetic fields to the neutron optical potentials, trapping of UCNs can become strongly spin dependent. The trapping potential of the converter vessel shown in Fig. 1 is given by

$$V_{\rm trap} = \min[(V \pm V_{{\rm m}R} - V_{\rm He})\Theta(V \pm V_{{\rm m}R} - V_{\rm He}), \\ (\widetilde{V} - V_{\rm He})\Theta(\widetilde{V} - V_{\rm He})], \tag{7}$$

i.e., the minimum of the total potential (neutron optical wall potential and magnetic interaction potential, reduced by the neutron optical potential of the converter medium). The first argument describes the situation at the cylindrical wall (with potential V), the second one at the end disks (potential $\widetilde{V} \geqslant V$). The expression employs the step function $\Theta(x) = 1$ for $x > 0$ and $\Theta(x) = 0$ for $x \leqslant 0$, and

$$V_{\rm He} \approx 18.5 \text{ neV} \tag{8}$$

is the neutron optical potential of the superfluid ^{4}He as calculated by using Eq. (4) with $N_{\rm He} \approx 2.18 \times 10^{22}$ cm^{-3} and $b_{\rm He} \approx 3.26 \times 10^{-13}$ cm. For the lfs neutrons the lowest potential energy prevails on the line $r = 0$, whereas for the hfs neutrons it has its minimum close to the cylindrical wall (see Fig. 2). Note however that the hfs neutrons will only be able to leave the magnetic field if they still possess kinetic energy at $r = 0$ and hence only for $\epsilon_0 > V_{{\rm m}R}$ according to our previous definition of ϵ_0. Since we are not further interested in the fate of hfs neutrons unable to escape the multipolar field after opening the UCN valve, and for simplicity of the equations to follow, we define ϵ_0 in the sequel commonly for both spin states as the kinetic energy at the point of lowest magnetic field (i.e., on the line $r = 0$). Equation (3) thus describes, individually for both spin states, UCN densities of usable UCNs (i.e., those with $\epsilon_0 > 0$), with $V_{\rm trap}$ as defined in Eq. (7). We define the polarization of the saturated ensemble of usable UCNs as

$$P_\infty = \frac{n_{\infty,{\rm lfs}} - n_{\infty,{\rm hfs}}}{n_{\infty,{\rm lfs}} + n_{\infty,{\rm hfs}}}. \tag{9}$$

surface of wall material exposed to the UCNs during accumulation. Here we analyze the system as shown in Fig. 1.

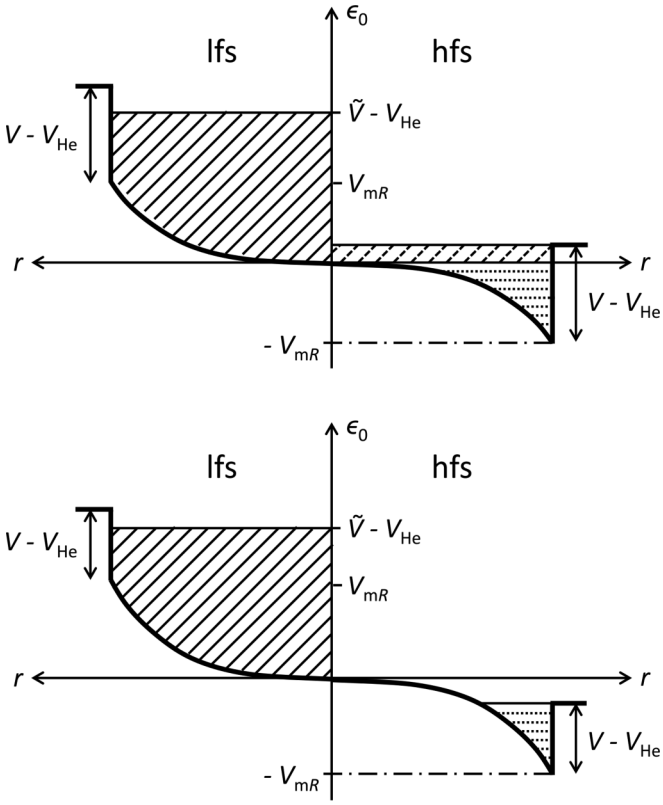

FIG. 2. Schematic of the magnetic and neutron optical potentials in the closed UCN accumulator shown in Fig. 1. In the upper figure, $V - V_{\mathrm{He}} > V_{\mathrm{m}R}$. Low-field-seeking (lfs) UCNs with total energy $\epsilon_0 < \widetilde{V} - V_{\mathrm{He}}$ are trapped (solid-line shade). High-field-seeking (hfs) UCNs with $0 < \epsilon_0 < V - V_{\mathrm{He}} - V_{\mathrm{m}R}$ are trapped, too (dashed-line shade), leading to polarization $P_\infty < 1$ according to Eq. (9). The lower figure illustrates the situation $V - V_{\mathrm{He}} < V_{\mathrm{m}R}$ where hfs UCNs with $\epsilon_0 > 0$ are free to escape, hence $P_\infty = 1$. Only hfs UCNs with $\epsilon_0 < 0$ (horizontal dotted shade) are trapped which, however, will stay in the regions with strong magnetic field when opening the UCN valve.

As shown in Fig. 2 for two situations it will depend on the relative strengths of magnetic and neutron optical potentials.

III. ULTRACOLD NEUTRON LOSSES FROM THE CONVERTER

The inverse of the time constant appearing in the loss term in Eq. (1) is comprised of several contributions,

$$\tau^{-1}(\epsilon_0, T) = \tau_{\mathrm{wall}}^{-1}(\epsilon_0) + \tau_{\mathrm{slit}}^{-1}(\epsilon_0) + \tau_{\mathrm{up}}^{-1}(T) + \tau_{\mathrm{abs}}^{-1} + \tau_{\mathrm{depol}}^{-1}(\epsilon_0) + \tau_\beta^{-1}, \tag{10}$$

where the argument indicates now also the dependence on the temperature T of the converter. From left to right, they describe UCN loss at collisions with the walls of the converter vessel, escape of UCNs through an imperfectly closed UCN valve and through slits caused by manufacturing imperfections of the vessel assembly, upscattering by thermal excitations in the helium, absorption by ^{3}He impurities, UCN depolarization at wall collisions, and neutron beta decay. Note that, when using an unpolarized beam for neutron conversion, the rate constant $\tau_{\mathrm{depol}}^{-1}$ may become relevant only if trapping is at least partly magnetic. In an experimental study a depolarization probability per wall collision of 7×10^{-6} was measured for a bottle made of Be [72]. Hence, $\tau_{\mathrm{depol}}^{-1} < \tau_\beta^{-1}$ even for the fastest neutrons in the narrow trap geometry discussed here. Like the first two rate constants in Eq. (10), $\tau_{\mathrm{depol}}^{-1}$ will be further suppressed due to the multipole magnet (provided that spin transport is adiabatic), and we therefore neglect it. For temperatures below 1 K [69,73],

$$\tau_{\mathrm{up}}^{-1}(T) \approx \frac{(T[\mathrm{K}])^7}{100\ \mathrm{s}}, \tag{11}$$

so that for $T < 0.5$ K, τ_{up}^{-1} contributes with less than 10% of τ_β^{-1}. The rate constant τ_{abs}^{-1} can be suppressed below any relevant level by purification of the helium from ^{3}He using a superleak [61,74,75] or the heat-flush technique [76]. As a result, we are left with $\tau_{\mathrm{wall}}^{-1}$ and $\tau_{\mathrm{slit}}^{-1}$ as dominating contributions, and the rate constant due to neutron decay sets an ultimate lower limit for a perfect converter.

For losses due to wall collisions we want to apply an analytic description. If we assume the trapped UCNs in mechanical equilibrium we can use formulas derived in the book [4] where the authors analyzed the effect of Earth's gravitational field on neutrons moving in a bottle. We adapt the notation to our case and replace the height parameter h by the radial coordinate r characterizing the multipolar magnetic field strength. We neglect the gravitational field, which is a good approximation for a horizontal source with less than 10 cm diameter. The kinetic neutron energy for the two spin states is then given by $E(r) = \epsilon_0 \mp |V_{\mathrm{m}}(r)|$. The energy

$$E := E(R) = \epsilon_0 \mp V_{\mathrm{m}R} \tag{12}$$

is positive for the extractable hfs neutrons which can always explore the whole trap. The low-field-seeking neutrons on the other hand may have too low energy to hit the walls. For $E > 0$ Eq. (12) defines the energy of neutron impact. Employing a formula given in Ref. [4], the angular-averaged probability $\overline{\mu}(E)$ for UCN loss during a collision with the cylindrical wall of the helium-filled converter vessel can be written as

$$\overline{\mu}(E) = 2f\mathrm{Re}\left(\frac{V'}{E}\arcsin\sqrt{\frac{E}{V'}} - \sqrt{\frac{V'}{E} - 1}\right) \quad \text{for} \quad E \leqslant V', \tag{13}$$

valid for a neutron optical potential $V + iW$ with small losses, i.e., ($f = W/V \ll 1$, and writing

$$V' = V - V_{\mathrm{He}}, \tag{14}$$

with V_{He} given in Eq. (8). For convenience in later calculations we have included a projection onto the real part of the expression. It offers a handy formulation of the case where neutrons have too low energy to hit the wall, ensuring that $\overline{\mu}(E < 0) = 0$ without need to specify the range of E in advance as positive. The function $\overline{\mu}(E)$ rises monotonically with E from $\overline{\mu} = 0$ for $E = 0$ to $\overline{\mu} = \pi f$ for $E = V'$. For $E > V'$ we may set $\overline{\mu} = 1$ since we are not interested here in calculating the dynamics of marginally trapped neutrons. For

TABLE I. Values for γ' for low-field-seeking neutrons, as defined with the upper sign in Eq. (18), for various values of ϵ_0/V_{mR}.

n	$\frac{\epsilon_0}{V_{mR}}$						
	$\frac{1}{10}$	$\frac{1}{5}$	$\frac{1}{2}$	1	$\frac{4}{3}$	$\frac{8}{5}$	2
4	0.005	0.021	0.133	0.533	0.696	0.758	0.813
6	0.067	0.133	0.333	0.667	0.778	0.822	0.862
8	0.159	0.252	0.465	0.739	0.824	0.859	0.89
10	0.248	0.351	0.555	0.785	0.855	0.883	0.909
12	0.325	0.429	0.619	0.818	0.876	0.9	0.922
14	0.39	0.492	0.667	0.841	0.892	0.913	0.932

$E = V'/2$, $\overline{\mu} \approx 1.14 f$. Note that, since we consider a long trap for which $2\pi RL \gg \pi R^2$, we will neglect losses due to $\widetilde{W}$ at the end disks. The magnetic multipole suppresses wall losses of lfs UCNs for several reasons. First, only a fraction of them has sufficient energy to hit the lossy wall. Second, those lfs neutrons with $\epsilon_0 > V_{mR}$ hit the wall due to magnetic deceleration with a reduced kinetic energy E [Eq. (12)], leading to reduced losses due to $\overline{\mu}(\epsilon_0 - V_{mR}) < \overline{\mu}(\epsilon_0)$. Third, the rate of wall collisions of these neutrons is reduced as well, leading to a further suppression in the expressions for τ_{wall}^{-1} and τ_{slit}^{-1}, which we calculate next.

In mechanical equilibrium, a group of neutrons with total energy in the range $(\epsilon_0, \epsilon_0 + d\epsilon_0)$ will occupy the accessible phase space in the trap with uniform density. As a result of phase space transformation under the influence of a conservative potential (see section 4.3.1 in Ref. [4]), the real space spectral UCN densities in different positions are related by

$$n(\epsilon_0,t,r) = \mathrm{Re}\sqrt{\frac{\epsilon_0 \mp |V_m(r)|}{\epsilon_0}}\, n(\epsilon_0,t,0), \tag{15}$$

where projection onto the real part ensures $n(\epsilon_0,t,r) = 0$ for the lfs UCNs for $r > R^*$ defined by $\epsilon_0 = |V_m(R^*)|$. We define an effective volume of the source for neutrons with total energy ϵ_0 as

$$\gamma(\epsilon_0) = 2\pi L \mathrm{Re}\int_0^R \sqrt{\frac{\epsilon_0 \mp |V_m(r)|}{\epsilon_0}}\, r dr. \tag{16}$$

The spectral UCN density averaged over the entire volume of the converter is then given by

$$n(\epsilon_0,t) = \gamma'(\epsilon_0) n(\epsilon_0,t,0), \tag{17}$$

and the reduced quantity

$$\gamma'(\epsilon_0) = \frac{\gamma(\epsilon_0)}{\pi R^2 L} = 2\mathrm{Re}\int_0^1 \sqrt{1 \mp \frac{V_{mR}}{\epsilon_0} r^{\frac{n}{2}-1}}\, r dr \tag{18}$$

was derived by using Eq. (6). Values for γ' listed in Table I show that, the higher the multipolarity, the less significant becomes the reduction of the density of the lfs neutrons with respect to a square-well potential of same depth. The spectral current density of neutrons at any point in the vessel, per unit area and per energy interval about ϵ_0, is given by the gas kinetic relation

$$J(\epsilon_0,t,r) = \tfrac{1}{4} n(\epsilon_0,t,r) v(\epsilon_0,r). \tag{19}$$

The spectral rate of UCN collisions with the cylindrical wall of the helium container is given by $2\pi RL J(\epsilon_0,t,R)$. The speed $v(\epsilon_0,R)$ of the neutrons as they hit the wall is related to the speed at $r = 0$ through

$$v(\epsilon_0,R) = \mathrm{Re}\sqrt{\frac{\epsilon_0 \mp V_{mR}}{\epsilon_0}}\, v(\epsilon_0,0). \tag{20}$$

With Eq. (15) we obtain

$$J(\epsilon_0,t,R) = \frac{\epsilon_0 \mp V_{mR}}{\epsilon_0} J(\epsilon_0,t,0)\Theta(\epsilon_0 \mp V_{mR}), \tag{21}$$

with the step function $\Theta(x)$ as already used in Eq. (7). For the loss term in Eq. (1) due to collisions with the cylindrical wall we can thus write

$$\frac{n(\epsilon_0,t)}{\tau_{wall}(\epsilon_0)} = \frac{2}{R}\overline{\mu}(\epsilon_0 \mp V_{mR}) J(\epsilon_0,t,R). \tag{22}$$

Further evaluation using Eq. (21), Eq. (19) for $r = 0$, Eq. (17), and inserting $\overline{\mu}$ from Eq. (13) leads us to

$$\tau_{wall}^{-1}(\epsilon_0) = \frac{v(\epsilon_0,0)}{R\gamma'(\epsilon_0)} f \frac{V'}{\epsilon_0} \mathrm{Re}\left[\arcsin\sqrt{\frac{\epsilon_0 \mp V_{mR}}{V'}} - \sqrt{\frac{\epsilon_0 \mp V_{mR}}{V'}\left(1 - \frac{\epsilon_0 \mp V_{mR}}{V'}\right)}\right]. \tag{23}$$

For the calculation of the corresponding expression for losses through slits it is reasonable to assume them to be situated at $r = R$, e.g., at the seam of the tube or at its connections to the circular windows for the cold beam. Assuming that any UCN hitting a slit will be lost and denoting the total surface of all slits by A, their contribution to the loss term in Eq. (1) is given by

$$\frac{n(\epsilon_0,t)}{\tau_{slit}(\epsilon_0)} = \frac{2}{R}\frac{A}{2\pi RL} J(\epsilon_0,t,R), \tag{24}$$

neglecting the small surface of the disks at the ends. Hence,

$$\tau_{slit}^{-1}(\epsilon_0) = \frac{A v(\epsilon_0,0)}{4\gamma(\epsilon_0)} \frac{\epsilon_0 \mp V_{mR}}{\epsilon_0} \Theta(\epsilon_0 \mp V_{mR}), \tag{25}$$

and we see that, for the lfs neutrons, the ordinary gas kinetic expression represented in the first fraction on the right side becomes reduced for $V_{mR} > 0$ for the same reason as the wall losses discussed before.

IV. ULTRACOLD NEUTRON PRODUCTION

We first consider UCN production in absence of the magnetic multipole field. For homogeneous irradiation with the cold-neutron beam guided through the converter, neglecting decrease of intensity due to reflection losses and neutron scattering in the helium, the UCN production rate density is position independent and given by

$$p_0 = \int_0^{V_{trap}} p_0(\epsilon_0) d\epsilon_0 = K V_{trap}^{3/2}. \tag{26}$$

The $V_{\rm trap}^{3/2}$ dependence follows for a homogeneous population of states within a sphere in momentum space with spectral UCN production rate density

$$p_0(\epsilon_0) = \frac{3}{2} K \sqrt{\epsilon_0}. \tag{27}$$

The factor K due to single-phonon emission has been calculated on the basis of neutron scattering data and confirmed in several experiments [62,77–82], albeit with modest experimental accuracy limited by detection efficiency and other corrections. For UCNs with maximum energy determined by $V_{\rm trap} = V - V_{\rm He} \approx 233$ neV for Be or Ni with natural isotopic composition, it is given by

$$K \approx (5\ {\rm s}^{-1}\,{\rm cm}^{-3})\Phi_{0.89\,{\rm nm}}[10^9\ {\rm cm}^{-2}\,{\rm s}^{-1}\,{\rm nm}^{-1}]/(233\ {\rm neV})^{3/2}, \tag{28}$$

where $\Phi_{0.89\,{\rm nm}}$ is the differential unpolarized neutron flux density at a neutron wavelength of 0.89 nm. The flux unit is chosen numerically close to values available at existing facilities, e.g., the monochromatic beam H172A at the ILL [47]. An additional, usually smaller contribution to UCN production is due to multiphonon processes.

When adding the multipolar magnetic field, the spectral UCN production rate density becomes dependent on position and spin state,

$$p_{\rm lfs(hfs)}(\epsilon_0, r) = \tfrac{3}{4} K(r) {\rm Re}\sqrt{\epsilon_0 \mp |V_m(r)|}, \tag{29}$$

where the r dependence of K accounts for a spatially varying flux density of the neutron beam. The factor $1/2$ with respect to Eq. (27) holds for an unpolarized beam incident on the converter, as always assumed hereafter. For homogeneous irradiation, $K(r) = K$, and the spatially averaged spectral UCN production rate density for the two spin states can be expressed in terms of the normalized effective volume from Eq. (18), i.e.,

$$p_{\rm lfs(hfs)}(\epsilon_0) = \tfrac{3}{4} K \gamma'(\epsilon_0) \sqrt{\epsilon_0}. \tag{30}$$

Without magnetic field, $p_{0,\rm lfs} = p_{0,\rm hfs} = p_0/2$ with p_0 given in Eq. (26), whereas with field,

$$p_{\rm lfs(hfs)} = \int_0^{V_{\rm trap}} p_{\rm lfs(hfs)}(\epsilon_0) d\epsilon_0 \tag{31}$$

are different due to the spin-dependent $\gamma'(\epsilon_0)$ and $V_{\rm trap}$ from Eq. (7). We note particularly that the ratio of total production rates for lfs UCNs with the magnetic multipole switched on and switched off,

$$\kappa = \frac{p_{\rm lfs}}{p_{0,\rm lfs}}, \tag{32}$$

is smaller than unity due to the phase space reduction by the magnetic multipole. The values quoted in Table II demonstrate a positive effect of high multipolar order n on κ and hence on the saturated UCN density calculated in the next section. There are, however, practical limits. First, thermal insulation between the magnet and the much colder helium container necessitates an annular gap over which the field would drop too strongly if n is chosen too large. Second, the maximum field strength achievable with a given maximum current density in the current bars around the converter of given diameter decreases with n. For $R = 5$ cm, and taking into account the results given in the next section, $n \approx 12$ turns out to be a reasonable choice.

TABLE II. Values for κ as defined in Eq. (32) for various values of n and $V_{{\rm m}R}/V_{\rm trap}$.

n	$\frac{V_{{\rm m}R}}{V_{\rm trap}}$			
	1	$\frac{3}{4}$	$\frac{5}{8}$	$\frac{1}{2}$
4	0.229	0.37	0.456	0.551
6	0.4	0.517	0.585	0.659
8	0.512	0.609	0.665	0.725
10	0.589	0.672	0.72	0.77
12	0.645	0.718	0.759	0.802
14	0.688	0.752	0.788	0.827

V. SATURATED ULTRACOLD NEUTRON DENSITY

The spatially averaged saturated spectral densities for lfs and hfs UCNs follow from Eq. (2) with Eq. (30), i.e.,

$$n_{\infty,\rm lfs(hfs)}(\epsilon_0) = \tfrac{3}{4} K \gamma'(\epsilon_0) \sqrt{\epsilon_0} \tau(\epsilon_0), \tag{33}$$

using the corresponding sign in Eqs. (18) and in the expression for $\tau(\epsilon_0)$. Hence, upon using Eq. (3) and writing out all arguments relevant for characterizing the multipolar magnetic field and the converter, the saturated total mean UCN densities in the converter are given by

$$n_{\infty,\rm lfs(hfs)}(R, V_{{\rm m}R}, n, V, f, \widetilde{V}, T) = \frac{3}{4} K \int_0^{V_{\rm trap}} \frac{\gamma'(\epsilon_0, V_{{\rm m}R}, n)\sqrt{\epsilon_0}}{\tau^{-1}(\epsilon_0, R, V_{{\rm m}R}, n, V, f, T)} d\epsilon_0. \tag{34}$$

The dependence on $\widetilde{V}$ is contained in the upper limit of integration; see Eq. (7). From the various contributions to the rate constant τ^{-1} [see Eq. (10)] we retain the terms due to wall collisions, upscattering [Eq. (11)] and neutron beta decay, assuming that the wall losses can entirely be described by Eq. (23) and that there is no ^{3}He in the converter and no slit in the vessel.

A first calculation of $n_{\infty,\rm lfs}$ and $n_{\infty,\rm hfs}$ was performed for a vessel featuring the neutron optical potential of Be at all walls (i.e., $\widetilde{V} = V = 252$ neV). Beryllium has become a standard material for UCN trapping, with a best reported experimental value of $f = 3 \times 10^{-5}$ in the low-temperature limit [83,84], despite a much smaller theoretical value (the finding that this was never reached was termed "anomalous losses" and has triggered many experimental investigations and speculations). However, it might be more realistic to consider also worse values for f, assuming that efficient cleaning procedures cannot be applied *in situ* (e.g., baking is excluded in presence of indium seals). Figure 3 shows results exemplary for multipole orders $n = 8$ and $n = 12$ as a function of the magnetic trapping potential at the cylindrical wall of the vessel, normalized to the trapping depth without magnetic field. The density of lfs UCNs increases with n as expected due to the increase in trapping phase space, while that of the hfs neutrons decreases. Hence, for partial magnetic trapping of the lfs

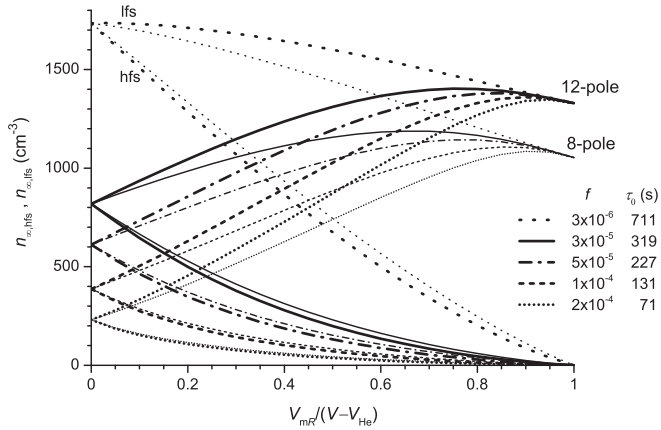

FIG. 3. Saturated densities of low-field-seeking and high-field-seeking UCNs in a converter vessel with diameter 10 cm held at 0.5 K and surrounded by a 12-pole and 8-pole magnet, respectively. Calculations employ Eq. (34) for $\widetilde{V} = V = 252$ neV (e.g., for a converter vessel made entirely of Be), and for various values of $f = W/V$. The solid lines show results for the best value of f previously achieved for Be, while the upmost curves show the situation for unrealistically low f for illustration. Values are given for an unpolarized differential neutron flux density of $\Phi_{0.89\,\mathrm{nm}} = 10^9\ \mathrm{cm^{-2}\,s^{-1}\,nm^{-1}}$ at $\lambda = 0.89$ nm, as available at the monochromatic beam position H172A at the ILL. A characteristic time constant τ_0 is calculated for neutrons with velocity $v = \frac{3}{4}v_{\max}$, including in Eq. (10) the rates τ_β^{-1}, τ_{up}^{-1}, and the wall collisional losses calculated using Eq. (23) for $V_{\mathrm{m}R} = 0$ and $\epsilon_0 = \frac{9}{16}V_{\mathrm{trap}}$.

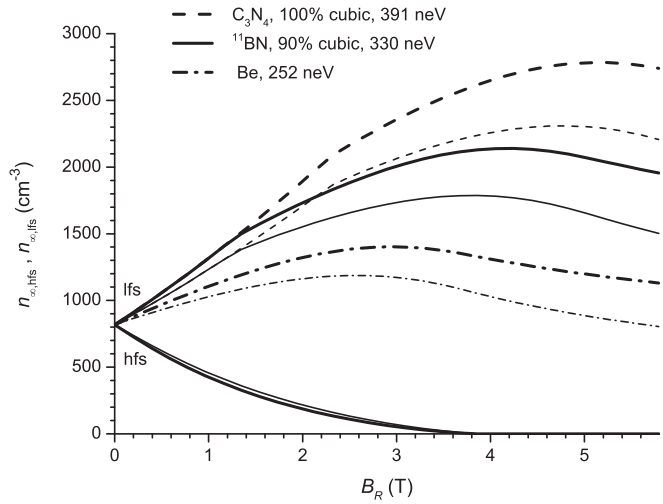

FIG. 4. Saturated densities of low-field-seeking and high-field-seeking UCNs in converter vessels with diameter 10 cm, $V = 252$ neV, $f = 3 \times 10^{-5}$, $T = 0.5$ K, and beam window and UCN valve (see Fig. 1) coated with three different materials with values of $\widetilde{V}$ as indicated in the legend. The thicker of each pair of curves is for multipolarity $n = 12$, the thinner is for $n = 8$, and all values are given for $\Phi_{0.89\,\mathrm{nm}} = 10^9\ \mathrm{cm^{-2}\,s^{-1}\,nm^{-1}}$ (unpolarized). The kinks visible for the two upper pairs of curves appear at field values corresponding to $V_{\mathrm{m}R} = \widetilde{V} - V$. Densities of the hfs UCNs for $\widetilde{V} \geqslant V$ are independent of $\widetilde{V}$ but are smaller for the higher multipole order.

neutrons (characterized by $V_{\mathrm{m}R} < V - V_{\mathrm{He}}$, see Fig. 2), higher multipole order leads to higher UCN polarization defined in Eq. (9). For instance, for a 12-pole magnet with $B_{\mathrm{R}} = 2.5$ T, one obtains $P_\infty = 86\%$ for $f = 3 \times 10^{-5}$ while for a worse $f = 2 \times 10^{-4}$ it improves to $P_\infty = 97\%$. As also obvious from the curves, the poorer the neutron optical UCN storage performance, the larger will be the improvement of lfs UCN density due to the multipole magnet. For the experimental cases reported in the introduction, with measured loss rate ratios as high as $\tau^{-1}/\tau_\beta^{-1} \simeq 5.5$ [39] and 13 [60], respectively, a multipole magnet would indeed be very useful. Some of the curves for $n_{\infty,\mathrm{lfs}}$ exhibit a maximum for values $V_{\mathrm{m}R}/V_{\mathrm{trap}} < 1$. This can be understood as resulting from the competition of storage-time constant τ and the effective trap volume γ' entering Eq. (34). For bad values of f the optimum obtains for $V_{\mathrm{m}R}/V_{\mathrm{trap}}$ close to 1, while for a trap with excellent storage properties the multipole field reduces the UCN density even at low field values because the factor $\gamma' < 1$ then dominates over a marginal gain in τ. For illustration of this behavior we also added a curve for an unrealistic converter vessel with hypothetical $f = 3 \times 10^{-6}$.

Next we consider an interesting further opportunity for buildup of a high lfs UCN density which takes advantage of the fact that the multipole magnet increases not only storage-time constants but also the potential energy of the neutron at the cylindrical wall. As a result, the trapping depth of the converter vessel becomes larger if the disks providing axial confinement are made of a material with larger neutron optical potential $\widetilde{V} > V$ (remember Eq. (7) and see Fig. 1). Since the surface of the disks is small, one may even employ materials which would be unsuitable for the entire vessel, for an unfavorably large $\widetilde{f} = \widetilde{W}/\widetilde{V}$ or because coating the tubular section with sufficient quality might be unavailable. While diamond-like carbon has already been studied in some detail [85–88], further candidate materials able to extend the spectrum for UCN trapping beyond the Be cutoff have been the scope of recent investigations [89]. Particularly promising is boron nitride in the cubic phase (cBN). Its neutron optical potential of 324 neV is even larger than that of diamond (304 neV) but due to the large absorption cross section of the isotope ^{10}B, $\widetilde{f} = 1.5 \times 10^{-2}$ is also excessively large. Enrichment of the weakly absorbing ^{11}B, however, may reduce $\widetilde{f}$ down to 3.3×10^{-5}, along with a further increase of $\widetilde{V}$ to a theoretical value of 351 neV. Using experiments on transmission with time-of-flight analysis and cold neutron reflectometry, the authors of Ref. [89] demonstrated a value of 305 ± 15 neV for their 2-μm-thick deposit of cBN (with natural isotopic composition) on a circular silicon waver. The deviation from the ideal value is due to a cubic phase content of 90%, which was measured independently by infrared spectroscopy. For highly enriched material, and assuming the same cubic phase content, one may expect a neutron optical potential of about 330 neV.

Figure 4 shows saturated UCN densities calculated for a trap with a Be-coated cylindrical wall with $f = 3 \times 10^{-5}$ and with the axial UCN confinement provided by Be, ^{11}BN (90% cubic), or cubic C_3N_4. The latter features an extraordinarily large theoretical value of $\widetilde{V} = 391$ neV. The curves for $\widetilde{V} > V$ for the lfs UCNs start with a slope larger than in the case

$\widetilde{V} = V$ (dash-dotted curve). This is due to a B_R-dependent increase of the integration range, $V_{\rm trap}$, in Eq. (34), as long as $V_{{\rm m}R} < \widetilde{V} - V$. Kinks in the curves appear at magnetic-field values corresponding to $V_{{\rm m}R} = \widetilde{V} - V$ where the full trapping depth is reached. While for a high-quality Be trap with $\widetilde{V} = V = 252$ neV the gain in UCN density is not too impressive (lowest two curves), for $\widetilde{V} = 330$ neV a magnetic 12 -pole with $B_R = 2.5$ T enhances the saturated low field seeker UCN density $n_{\infty,{\rm lfs}}$ by a factor 2.3 from 820 to 1880 cm^{-3}. Hence, if the experiment connected to the source can use the high-energy UCNs it provides, the magnetic multipole is an asset even for a vessel with very good storage properties. Note that the saturated high-field-seeker-UCN density $n_{\infty,{\rm hfs}}$ for $\widetilde{V} \geqslant V$ does not depend on $\widetilde{V}$, since for them the trapping potential is given by $V - V_{{\rm m}R}$ (see upper part of Fig. 2). Hence, the larger $\widetilde{V}$, the larger will be the polarization P_∞ defined in Eq. (9) (see also Table III). Note also that, as sketched in the lower part of Fig. 2, for magnetic fields providing a trapping potential stronger than the neutron optical potential ($B_R \gtrsim 3.9$ T for the situation shown in Fig. 4), $P_\infty = 1$.

Figure 5 shows the dependence of saturated UCN density on the multipole order for traps with a Be-coated cylindrical wall with $f = 3 \times 10^{-5}$, $f = 2 \times 10^{-4}$, each with end windows with a potential of $\widetilde{V} = 330$ neV. Again, one notes the positive influence of higher multipole order on the number of trapped UCN and on the polarization. Table III quotes values for $n_{\infty,{\rm lfs}}$ and P_∞ for $n = 12$ and for various values of f. One can see, for instance, for $f = 2 \times 10^{-4}$, that the magnetic field enhances $n_{\infty,{\rm lfs}}$ by more than a factor five from 230 to 1210 cm^{-3}. One also notes that the multipole field stabilizes the output of the source, by mitigating the influence of the loss coefficient of the converter wall surface. This includes possible deterioration of the wall quality with time, which will then also be much less an issue than without the field.

For application of the source for feeding a magnetic trap, e.g., for neutron-lifetime experiments with typical trapping potentials in the range 50 to 120 neV (see current projects in Refs. [63,90–93]), it is interesting to study the dependence of $n_{\infty,{\rm lfs}}$ on the upper bound of the trapped UCN energy spectrum. Figure 6 shows this dependence, for traps with $n = 12$ and again with the cylindrical section made of Be with $f = 3 \times 10^{-5}$, respectively $f = 2 \times 10^{-4}$. Values are calculated using Eq. (34) with the potential $\widetilde{V} - V_{\rm He}$ set to different values starting from 60 neV and increased in steps of 20 neV. We see that, the lower $\widetilde{V}$, the lower will be the magnetic field needed to optimize the UCN density. The reason is that lowering $\widetilde{V}$ reduces wall collisional losses due to the energy dependence of $\overline{\mu}(E)$ defined in Eq. (13) and due to wall hits occurring at a smaller rate, whereas the effective volume γ' decreases quickly with $V_{{\rm m}R}$ for a low-energy UCN spectrum (see Table I). The solid curves in Fig. 6 tell us that, for the converter vessel coated with an excellent Be mirror, $f = 3 \times 10^{-5}$, the multipole magnet will offer some advantage only for not-too-low UCN cutoff energy. However, for a more realistic situation, $f = 2 \times 10^{-4}$, gains due to the magnet are rather significant even for low-energy UCN spectra. For example, for feeding an external trap with trapping depth 60 neV, it will improve $n_{\infty,{\rm lfs}}$ by a factor 2 at $B_R \approx 0.8$ T. With increasing trapping depth the gain increases, e.g., to a factor 3.2 at $B_R \approx 1.8$ T for $V_{\rm trap} = 120$ neV.

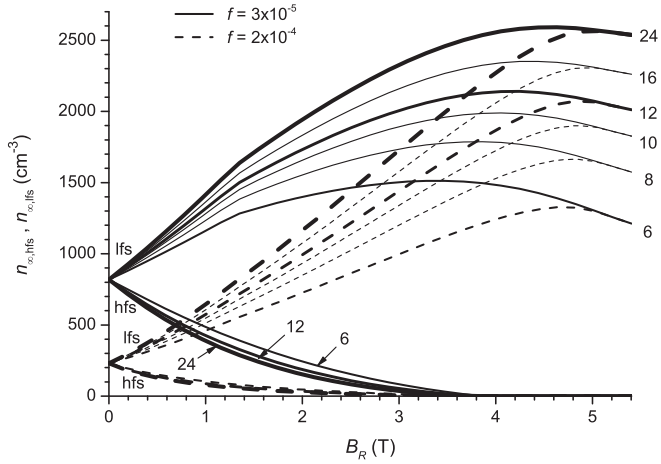

FIG. 5. Saturated densities of low-field-seeking and high-field-seeking UCNs in converter vessels with diameter 10 cm, $V = 252$ neV, $T = 0.5$ K, $f = 3 \times 10^{-5}$ (solid curves) or $f = 2 \times 10^{-4}$ (dashed curves). Beam window and UCN valve (see Fig. 1) are coated with $C^{11}BN$ with $\widetilde{V} = 330$ neV. The magnetic multipole order is varied between $n = 6$ and 24. Values are given for $\Phi_{0.89\,{\rm nm}} = 10^9$ cm^{-2} s^{-1} nm^{-1} (unpolarized).

VI. CONCLUSIONS

As our analysis shows, a multipole magnet can lead to a large gain in the saturated density of low-field-seeking UCNs because the presence of the field reduces the number

TABLE III. Values for the saturated density of low-field-seeking UCNs [see Eq. (34)] and UCN polarization [Eq. (9)], for a converter vessel with $R = 5$ cm, $T = 0.5$ K, surrounded by a 12-pole magnet, and for several values of f. Values are given for an unpolarized differential flux density of $\Phi_{0.89\,{\rm nm}} = 10^9$ cm^{-2} s^{-1} nm^{-1}.

$\widetilde{V}$ (neV)	B_R (T)		f			
			3×10^{-5}	1×10^{-4}	2×10^{-4}	4×10^{-4}
330	2.5	$n_{\infty,{\rm lfs}}$ (cm^{-3})	1880	1430	1210	1050
		P_∞	0.89	0.949	0.969	0.981
252	2.5	$n_{\infty,{\rm lfs}}$ (cm^{-3})	1380	1200	1080	980
		P_∞	0.86	0.939	0.965	0.98
$\geqslant$252	0	$n_{\infty,{\rm lfs}}$ (cm^{-3})	820	390	230	130
		P_∞	0	0	0	0

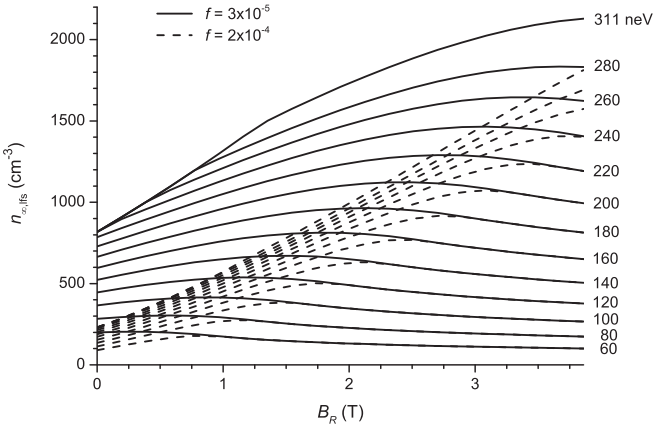

FIG. 6. Saturated density of low-field-seeking UCN in converter vessels with diameter 10 cm, $V = 252$ neV, $T = 0.5$ K, and surrounded by a 12-pole magnet. Solid curves are for $f = 3 \times 10^{-5}$, dashed ones for $f = 2 \times 10^{-4}$. $\widetilde{V} - V_{\mathrm{He}}$ is varied between 60 neV and 311 neV. Values are given for $\Phi_{0.89\,\mathrm{nm}} = 10^9\ \mathrm{cm^{-2}\,s^{-1}\,nm^{-1}}$ (unpolarized).

of neutrons hitting the material walls and reduces the energy and wall collision rate of those that do. In addition, it acts as a source-intrinsic UCN polarizer without need to polarize the incident beam and hence avoiding associated losses. A 12-pole magnet with field $B_R = 2.5$ T on a radius of $R = 5$ cm seems technically feasible using standard NbTi-superconducting-wire technology, as investigated in an independent study using a finite-element code. Based on results of experimental work done by other groups, a promising candidate vessel able to provide a UCN spectrum with exceptionally high cutoff consists of a Be trap closed off by disks coated with $C^{11}BN$. Alternative materials are diamond-like carbon with V close to 300 neV depending on the abundance of sp^3 chemical bonds, or enriched ^{58}Ni with $\overline{V} = 346$ neV and a theoretical $f = 8.6 \times 10^{-5}$, which, however, is magnetic so that UCN depolarization might be an issue that needs experimental study. We note that, in order to extract the full benefits, the incoming cold beam will need to be transported by a supermirror guide, with a top layer deposit of a good UCN reflecting material with neutron optical potential V. An experimental study of a UCN source prototype involving a converter vessel coated with such type of mirror is currently underway at the ILL, in preparation of the UCN source project SuperSUN which will include a 12-pole magnet around a 3-m-long cylindrical converter vessel.

Our benchmark converter is able to provide a saturated low-field-seeker UCN density almost as high as an unrealistic, perfect trap with $f = 0$ and Be cutoff, for which one calculates $n_{\infty,\mathrm{lfs}} = 2060\ \mathrm{cm^{-3}}$ when exposed to a neutron beam with differential flux density $\Phi_{0.89\,\mathrm{nm}} = 10^9\ \mathrm{cm^{-2}\,s^{-1}\,nm^{-1}}$. For a pure Be trap equipped with the 12-pole magnet one calculates $n_{\infty,\mathrm{lfs}} = 1380\ \mathrm{cm^{-3}}$ for $f = 3 \times 10^{-5}$ as previously achieved for this material, while for f ten-times worse, we still obtain $n_{\infty,\mathrm{lfs}} = 1110\ \mathrm{cm^{-3}}$. Without the magnet, on the other hand, $n_{\infty,\mathrm{lfs}}$ would get suppressed by a factor of five, which impressively demonstrates the capability of the magnetic multipole reflector to mitigate the influence of a poor loss coefficient f of the converter wall surface. Obviously, also if loss of quality of the inner converter surface with time will be an issue, the magnet offers a valuable practical advantage.

Including the high-field seekers into the discussion, one first notes that without magnetic field they are equally well trapped, so that in this case (and still assuming the usual situation of an unpolarized cold-neutron beam for UCN production) the total UCN density in the source will be a factor two higher. However, for experiments requiring polarized UCNs such as magnetic traps for precise determination of the neutron lifetime, or the neutron EDM experiment, this factor is of no use. Values for polarization of the trapped ensemble of UCNs after saturation of the source were quoted in Table III and are typically well beyond 90% for the system discussed. As obvious from Fig. 2, low-energy UCNs may stay poorly polarized whereas for the high-energy part of the spectrum the high-field seekers, after magnetic acceleration to the cylindrical wall, will have kinetic energy beyond its cutoff potential and quickly get lost. Poor polarization is not a problem for experiments using magnetic traps which can be designed for quick cleaning out the wrong spin component. For experiments that would profit from a very high initial polarization one might coat the converter vessel with a low-loss material with potential $V < V_{\mathrm{m}R}$, which would lead to nearly 100% UCN polarization since the high-field seekers would stay untrapped. For a system with $V > V_{\mathrm{m}R}$ one may still, if needed, increase the polarization by delayed extraction of the UCNs after having switched off the saturating neutron beam. The high-field seekers will then leave the trap more quickly than the low-field seekers due to shorter trapping time constants. One might also cut out the lowest-energy part of the spectrum by a vertical UCN guide section with suitably chosen length.

As an important detail not affecting our conclusions we note that, in addition to the multipole field, it will be necessary to apply a bias field on the order of some 10 mT along the converter axis to avoid depolarization in the region around $r = 0$, where the multipole field is zero. In addition, we can consider using axial magnetic pinch fields to increase V_{trap} and thereby the density of the UCNs for an extended energy spectrum. For extraction, the field at one end needs to be ramped down, so that an iris-type UCN valve might be most appropriate for this case. An extended UCN spectrum would be interesting if UCNs of any velocity were beneficial, such as in UCN transmission experiments, or in combination with a phase space transformation by letting the UCNs rise against the gravitational field. Note however that low-loss extraction of such a UCN spectrum will be a challenge. On the other hand, some studies might be performed *in situ* by using static pinch fields, such as experiments on UCN upscattering in superfluid ^{4}He, for which any increase in UCN density will be very welcome.

ACKNOWLEDGMENT

Funding of the UCN-source project SuperSUN by the French Agence nationale de la recherche (ANR) is gratefully acknowledged.

[1] E. Fermi, Ricerca Scientifica **7**, 13 (1936).
[2] V. I. Luschikov, Yu. N. Pokotilovsky, A. V. Strelkov, and F. L. Shapiro, Sov. Phys. JETP Lett. **9**, 23 (1969).
[3] A. Steyerl, Phys. Lett. B **29B**, 33 (1969).
[4] R. Golub, D. J. Richardson, and S. K. Lamoreaux, *Ultra-Cold Neutrons* (Adam Hilger, Bristol, 1991).
[5] V. K. Ignatovich, *The Physics of Ultracold Neutrons* (Oxford Science Publications, Clarendon Press, Oxford, 1990).
[6] D. Dubbers and M. G. Schmidt, Rev. Mod. Phys. **83**, 1111 (2011).
[7] M. J. Ramsey-Musolf and S. Su, Phys. Rep. **456**, 1 (2008).
[8] H. Abele, Prog. Part. Nucl. Phys. **60**, 1 (2008).
[9] T. Jenke, P. Geltenbort, H. Lemmel, and H. Abele, Nat. Phys. **7**, 468 (2011).
[10] A. P. Serebrov, E. B. Aleksandrov, N. A. Dovator *et al.*, Phys. Lett. B **663**, 181 (2008).
[11] G. Ban, K. Bodek, M. Daum *et al.*, Phys. Rev. Lett. **99**, 161603 (2007).
[12] I. Altarev, C. A. Baker, G. Ban *et al.*, Phys. Rev. Lett. **103**, 081602 (2009).
[13] T. Jenke, G. Cronenberg, J. Burgdörfer *et al.*, Phys. Rev. Lett. **112**, 151105 (2014).
[14] A. P. Serebrov, O. Zimmer, P. Geltenbort *et al.*, JETP Lett. **91**, 6 (2010).
[15] O. Zimmer, Phys. Lett. B **685**, 38 (2010).
[16] A. I. Frank, P. Geltenbort, M. Jentschel *et al.*, Phys. At. Nucl. **71**, 1656 (2008).
[17] S. Filipp, J. Klepp, Y. Hasegawa, C. Plonka-Spehr, U. Schmidt, P. Geltenbort, and H. Rauch, Phys. Rev. Lett. **102**, 030404 (2009).
[18] D. J. Richardson and S. K. Lamoreaux, Nucl. Instrum. Methods Phys. Res., Sect. A **284**, 192 (1989).
[19] D. J. Richardson, A. I. Kilvington, K. Green, and S. K. Lamoreaux, Phys. Rev. Lett. **61**, 2030 (1988).
[20] T. Bitter and D. Dubbers, Phys. Rev. Lett. **59**, 251 (1987).
[21] S. S. Arzumanov *et al.*, JETP Lett. **95**, 224 (2012).
[22] A. Pichlmaier, V. Varlamov, K. Schreckenbach, and P. Geltenbort, Phys. Lett. B **693**, 221 (2010).
[23] S. Paul, Nucl. Instrum. Methods Phys. Res., Sect. A **611**, 157 (2009).
[24] A. P. Serebrov, V. E. Varlamov, A. G. Kharitonov *et al.*, Phys. Rev. C **78**, 035505 (2008).
[25] J. S. Nico, M. S. Dewey, D. M. Gilliam, F. E. Wietfeldt *et al.*, Phys. Rev. C **71**, 055502 (2005).
[26] M. P. Mendenhall, R. W. Pattie, Y. Bagdasarova *et al.*, Phys. Rev. C **87**, 032501 (2013).
[27] B. Plaster, R. Rios, H. O. Back, T. J. Bowles *et al.*, Phys. Rev. C **86**, 055501 (2012).
[28] D. Mund, B. Märkisch, M. Deissenroth, J. Krempel, M. Schumann, H. Abele, A. Petoukhov, and T. Soldner, Phys. Rev. Lett. **110**, 172502 (2013).
[29] H. Abele, S. Baessler, D. Dubbers *et al.*, Phys. Rev. Lett. **88**, 211801 (2002).
[30] A. Coc, N. J. Nunes, K. A. Olive, J.-P. Uzan, and E. Vangioni, Phys. Rev. D **76**, 023511 (2007).
[31] R. E. Lopez and M. S. Turner, Phys. Rev. D **59**, 103502 (1999).
[32] G. Mention, M. Fechner, Th. Lasserre, T. A. Mueller, D. Lhuillier, M. Cribier, and A. Letourneau, Phys. Rev. D **83**, 073006 (2011).
[33] E. M. Purcell and N. F. Ramsey, Phys. Rev. **78**, 807 (1950).
[34] M. Pospelov and A. Ritz, Ann. Phys. (NY) **318**, 119 (2005).
[35] C. A. Baker *et al.*, Phys. Rev. Lett. **97**, 131801 (2006).
[36] A. P. Serebrov, E. A. Kolomenskiy, A. N. Pirozhkov *et al.*, JETP Lett. **99**, 4 (2014) [Pis'ma v ZhETF **99**, 7 (2014)].
[37] I. Altarev *et al.*, Nuovo Cimento **35 C**, 122 (2012).
[38] Y. Masuda, K. Asahi, K. Hatanaka *et al.*, Phys. Lett. A **376**, 1347 (2012).
[39] M. G. D. van der Grinten, Nucl. Instrum. Methods Phys. Res., Sect. A **611**, 129 (2009).
[40] I. Altarev, G. Ban, G. Bison, K. Bodek *et al.*, Nucl. Instrum. Methods Phys. Res., Sect. A **611**, 133 (2009).
[41] A. P. Serebrov *et al.*, Nucl. Instrum. Methods Phys. Res., Sect. A **611**, 263 (2009).
[42] S. K. Lamoreaux and R. Golub, J. Phys. G **36**, 104002 (2009).
[43] The EDM@SNS neutron EDM experiment, http://p25ext.lanl.gov/edm/edm.html
[44] R. Golub and S. K. Lamoreaux, Phys. Rep. **237**, 1 (1994).
[45] J. Karch, Yu. Sobolev, M. Beck *et al.*, Eur. Phys. J. A **50**, 78 (2014).
[46] B. Lauss, Phys. Procedia **51**, 98 (2014).
[47] F. M. Piegsa, M. Fertl, S. N. Ivanov, M. Kreuz, K. K. H. Leung, P. Schmidt-Wellenburg, T. Soldner, and O. Zimmer, Phys. Rev. C **90**, 015501 (2014).
[48] T. Lauer and T. Zechlau, Eur. Phys. J. A **49**, 104 (2013).
[49] A. Saunders, M. Makela, Y. Bagdasarova *et al.*, Rev. Sci. Instrum. **84**, 013304 (2013).
[50] Y. Masuda, K. Hatanaka, S.-C. Jeong *et al.*, Phys. Rev. Lett. **108**, 134801 (2012).
[51] A. P. Serebrov, V. A. Mityuklaev, A. A. Zakharov *et al.*, Nucl. Instrum. Methods Phys. Res., Sect. A **611**, 276 (2009).
[52] E. I. Korobkina, B. W. Wehring, A. I. Hawari, A. R. Young *et al.*, Nucl. Instrum. Methods Phys. Res., Sect. A **579**, 530 (2007).
[53] A. Frei, Y. Sobolev, I. Altarev *et al.*, Eur. Phys. J. A **34**, 119 (2007).
[54] U. Trinks, F. J. Hartmann, S. Paul, and W. Schott, Nucl. Instrum. Methods Phys. Res., Sect. A **440**, 666 (2000).
[55] R. Golub and J. M. Pendlebury, Phys. Lett. A **53A**, 133 (1975).
[56] A. Serebrov *et al.*, J. Exp. Theor. Phys. **59**, 11 (1994).
[57] R. Golub and K. Böni, Z. Phys. B: Condens. Matter **51**, 95 (1983).
[58] I. Altarev *et al.*, Phys. Lett. A **80**, 413 (1980).
[59] A. I. Kilvington, R. Golub, W. Mampe, and P. Ageron, Phys. Lett. A **125**, 416 (1987).
[60] O. Zimmer, F. M. Piegsa, and S. N. Ivanov, Phys. Rev. Lett. **107**, 134801 (2011).
[61] O. Zimmer, P. Schmidt-Wellenburg, M. Fertl *et al.*, Eur. Phys. J. C **67**, 589 (2010).
[62] O. Zimmer, K. Baumann, M. Fertl *et al.*, Phys. Rev. Lett. **99**, 104801 (2007).
[63] K. Leung, S. Ivanov, F. Martin *et al.*, *Proceedings of the workshop "Next Generation Experiments to Measure the Neutron Lifetime," Santa Fe, New Mexico, 9–10 November 2012* (World Scientific, Singapore, 2014), pp. 145–154.
[64] K. K. H. Leung and O. Zimmer, Nucl. Instrum. Methods Phys. Res., Sect. A **611**, 181 (2009).
[65] O. Zimmer, J. Phys. G **26**, 67 (2000).
[66] P. R. Huffman, C. R. Brome, J. S. Butterworth *et al.*, Nature (London) **403**, 62 (2000).
[67] H. S. Sommers, J. G. Dash, and L. Goldstein, Phys. Rev. **97**, 855 (1955).
[68] J. Res., Natl. Inst. Stand. Technol. **110**, 339 (2005).

[69] R. Golub, C. Jewell, P. Ageron, W. Mampe, B. Heckel, and I. Kilvington, Z. Phys. B: Condens. Matter **51**, 187 (1983).
[70] K. K. H. Leung, Ph.D. thesis, TU Munich, 2013 (unpublished).
[71] V. F. Ezhov, A. Z. Andreev, A. A. Glushkov *et al.*, J. Res. Natl. Inst. Stand. Technol. **110**, 345 (2005).
[72] A. Serebrov *et al.*, Nucl. Instrum. Methods Phys. Res., Sect. A **440**, 717 (2000).
[73] R. Golub, Phys. Lett. A **72A**, 387 (1979).
[74] H. Yoshiki, H. Nakai, and E. Gutsmiedl, Cryogenics **45**, 399 (2005).
[75] H. Yoshiki, K. Sakai, T. Kawai, and S. Goto'o, Cryogenics **34**, 277 (1994).
[76] P. McClintock, Cryogenics **18**, 201 (1978).
[77] P. Schmidt-Wellenburg, K. H. Andersen, and O. Zimmer, Nucl. Instrum. Methods Phys. Res., Sect. A **611**, 259 (2009).
[78] C. A. Baker, S. N. Balashov, J. Butterworth *et al.*, Phys. Lett. A **308**, 67 (2003).
[79] E. Korobkina, R. Golub, B. W. Wehring, and A. R. Young, Phys. Lett. A **301**, 462 (2002).
[80] Y. Masuda, T. Kitagaki, K. Hatanaka *et al.*, Phys. Rev. Lett. **89**, 284801 (2002).
[81] P. Ageron, W. Mampe, R. Golub, and J. M. Pendlebury, Phys. Lett. A **66A**, 469 (1978).
[82] R. Golub and J. Pendlebury, Phys. Lett. A **82**, 337 (1977).
[83] T. Brys, M. Daum, P. Fierlinger *et al.*, Nucl. Instrum. Methods Phys. Res., Sect. A **551**, 429 (2005).
[84] V. Alfimenkov *et al.*, JETP Lett. **55**, 84 (1992).
[85] F. Atchison, B. Blau, M. Daum *et al.*, Nucl. Instrum. Methods Phys. Res., Sect. B **260**, 647 (2007).
[86] F. Atchison, B. Blau, M. Daum *et al.*, Phys. Rev. C **74**, 055501 (2006).
[87] F. Atchison, B. Blau, M. Daum *et al.*, Phys. Lett. B **642**, 24 (2006).
[88] M. G. D. van der Grinten, J. M. Pendlebury, D. Shiers *et al.*, Nucl. Instrum. Methods Phys. Res., Sect. A **423**, 421 (1999).
[89] Yu. Sobolev, Th. Lauer, Yu. Borisov *et al.*, Nucl. Instrum. Methods Phys. Res., Sect. A **614**, 461 (2010).
[90] V. F. Ezhov, A. Z. Andreev, G. Ban *et al.*, arXiv:1412.7434.
[91] D. J. Salvat, E. R. Adamek, D. Barlow *et al.*, Phys. Rev. C **89**, 052501 (2014).
[92] V. F. Ezhov, A. Z. Andreev, G. Ban *et al.*, Nucl. Instrum. Methods Phys. Res., Sect. A **611**, 167 (2009).
[93] R. Picker, I. Altarev, J. Bröcker *et al.*, J. Res. Natl. Inst. Stand. Technol. **110**, 357 (2005).